Coupled spin waves in trilayer films and nanostripes of permalloy separated by nonmagnetic spacers: Brillouin light scattering and theory

G. Gubbiotti,[1,2] S. Tacchi,[1,2] H. T. Nguyen,[3] M. Madami,[2,4] G. Carlotti,[2,5] K. Nakano,[6] T. Ono,[6] and M. G. Cottam[3]

[1]*Istituto Officina dei Materiali del CNR (CNR-IOM), Unità di Perugia, c/o Dipartimento di Fisica, Università di Perugia, I-06123 Perugia, Italy*

[2]*CNISM, Unità di Perugia and Dipartimento di Fisica, Università di Perugia, I-06123 Perugia, Italy*

[3]*Department of Physics and Astronomy, University of Western Ontario, London N6A 3K7, Canada*

[4]*Dipartimento di Fisica, Università di Perugia, I-06123 Perugia, Italy*

[5]*Istituto di Nanoscienze del CNR (CNR-NANO), Centro S3, Via Campi 213/A, 41125 Modena, Italy*

[6]*Laboratory of Nano Spintronics, Division of Materials Chemistry, Institute for Chemical Research, Kyoto University, Uji, Kyoto 611-0011, Japan*

(Received 29 December 2012; published 6 March 2013)

We present a combined experimental and theoretical study of the di-exchange spin waves in layered structures constituted by permalloy(30 nm)/Cu(10 nm)/permalloy (d)/Cu(10 nm)/permalloy (30 nm), which differ by the variable thickness d of the middle permalloy film (with $d = 15, 30, 60$ nm). Both the plane layered films and two sets of stripes having widths of 150 and 400 nm were studied. The spin-wave dispersions (frequency vs wave vector) were measured by Brillouin light scattering and the experimental data interpreted using a microscopic (Hamiltonian-based) theory that takes into account the magnetic dipole-dipole and exchange interactions within each stripe and the dipole-dipole coupling between stripes of the stack. Overall, good agreement is found, showing that modes of the layered films constituted by surface dipolar and exchange-dominated waves give rise to complicated spectra in the case of layered stripes because of the lateral confinement. The role of the middle-layer thickness d in the determination of the perpendicular profile of the spin modes is analyzed in detail.

DOI: 10.1103/PhysRevB.87.094406 PACS number(s): 75.30.Ds, 78.35.+c, 75.78.−n

I. INTRODUCTION

The study of the spin-wave properties in dipolarly coupled thin magnetic films dates back to the pioneering works of Grunberg,[1] where it has been shown that surface spin waves existing inside every magnetic film are coupled to one another via the long-range magnetic dipolar interaction, and the dynamic magnetization in the two layers can either precess in phase or out of phase by 180°. The investigation of magnetization dynamics of laterally confined elements composed of alternating ferromagnetic and nonmagnetic layers is a more recent research field,[2,3] the development of which is closely connected to the field of miniature magnetic sensors and information storage devices. To optimize and tailor technological applications, however, it is indispensable to understand the characteristics of the magnetic normal modes spectrum of these structures. It can be quite complex because of the interplay between shape anisotropy (arising from the lateral confinement), the asymmetry of the ferromagnetic layers (different thickness and/or different materials), the competing effects of short-range exchange, and long-range dipole-dipole interactions, as well as by the presence of external driving dynamics.[4–6]

Furthermore, although normal modes describe linear dynamics only (small-amplitude oscillations about the equilibrium state), they can be used to gain a physical understanding of nonlinear phenomena (large-amplitude oscillations) as well.[7] For instance, magnetization reversal is an example of a nonlinear process that has been interpreted on the basis of the profiles of the normal modes.[8]

Multilayered nanoelements with equal (e.g. permalloy/Cu/permalloy,[9–14] permalloy/Ru/permalloy,[15] and CoFeB/MgO/CoFeB[5,16]) and different magnetic materials (e.g. permalloy/Cu/Co[17–20]) with either almost uniform or vortex[21–24] magnetization ground state have been largely investigated as a function of different parameters, such as the element shape and dimensions, the magnetic field orientation/magnitude, and the interlayer thickness. In most cases, the thickness of the nonmagnetic spacer was larger than 5 nm in order to exclude interlayer exchange coupling between the ferromagnetic layers. In the case of identical magnetic materials, the spatial profiles of the modes in each layer showed a strong resemblance to the mode profiles in the corresponding isolated dots. This is because the dynamical dipolar coupling constitutes only a relatively weak perturbation of the individual resonances of the layers, and its principal effect is to introduce a fixed phase relation between the magnetization dynamics of the modes in the two layers. Oscillating modes, characterized by an in-phase or out-of-phase magnetization precession in the two magnetic layers, have been identified. Contrarily, for elements constituted by two different ferromagnetic materials, the calculated power spectra of the magnetic normal modes of individual elements are quite different, and so are the frequencies of the corresponding eigenmodes.

In this paper, we have measured, using the Brillouin light scattering (BLS) technique, the frequency dispersion (frequency vs wave vector) of thermally excited spin waves in permalloy(t)/Cu(d_0)/permalloy(d)/Cu(d_0)/permalloy(t) films and stripes, which differ due to the variable thickness d of the middle Py stripe (with $d = 15, 30, 60$ nm), while the thickness of the top and bottom permalloy layers and of the Cu spacer are kept fixed at $t = 30$ nm and $d_0 = 10$ nm, respectively.

In order to investigate the spatial quantization effects, two different stripe widths ($w_n = 150$ nm and $w_w = 400$ nm) have been studied. The purpose of this paper is to provide a comprehensive experimental and theoretical investigation of the dipole-exchange spin-wave modes existing in such layered structures. With respect to previous investigation of magnetic bilayers, the presence of a third magnetic layer with thickness $d = 15$, 30, and 60 nm, placed in the middle of the stack, introduces important modification in the spin-wave properties because it mediates the interlayer dipolar coupling between the outermost films and because perpendicular standing spin waves, dominated by exchange intralayer interaction, interact with the magnetostatic surface mode of dipolar nature. We stress that, while most of the previous studies were performed on micrometric-sized elements with small aspect ratios, where the approximation thickness/width $\ll 1$ is largely fulfilled, in this paper, we study the spin-wave modes in layered stripes with relatively large aspect ratio up to 0.4. This has important consequences on the magnetic normal modes of layered stripes which can have a resonant behavior along both the stripe width and thickness.

II. EXPERIMENT

Permalloy (Py) stripes were fabricated by a combination of e-beam lithography, RF sputtering, and lift-off process on thermally oxidized Si substrate. The stripes were arranged in arrays of dimensions of (800 × 800) μm^2 with edge-to-edge separation of 400 nm in order to exclude any significant interaction among the stripes. Both the continuous films and the stripes have the following layering scheme Py(t = 30 nm)/Cu(10 nm)/Py(d)/Cu(10 nm)/Py(t = 30 nm) and differ by the thickness of the middle Py stripe d (with $d = 15$, 30, 60 nm), as shown in Fig. 1. Two set of stripes, characterized by a different width of $w_n = 150$ nm (narrow) and $w_w = 400$ nm (wide), were studied and their scanning electron micrographs (SEM) images are reported in Fig. 2. The study of the continuous films, which can be considered as reference samples, is very useful for understanding the nature of the detected modes, i.e. bulk standing or surface modes, and to extract the values of the magnetic parameters by measuring the spin-wave dispersion. No appreciable in-plane dependence of magnetic properties has been observed for the trilayer films so that any magnetocrystalline anisotropy has been taken into account.

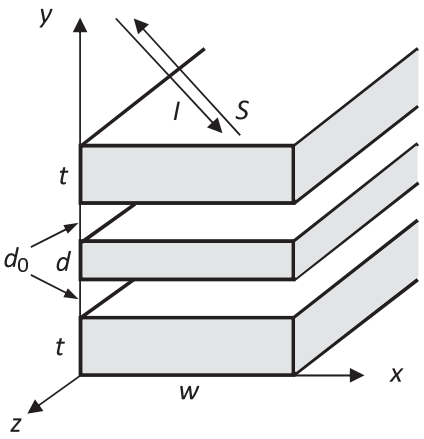

FIG. 1. The geometry of the trilayer structures of Py stripes separated by nonmagnetic Cu spacers of fixed thickness $d_0 = 10$ nm. Coordinate axes are shown, as well as the 180° backscattering geometry with incident (I) and scattered (S) light beams.

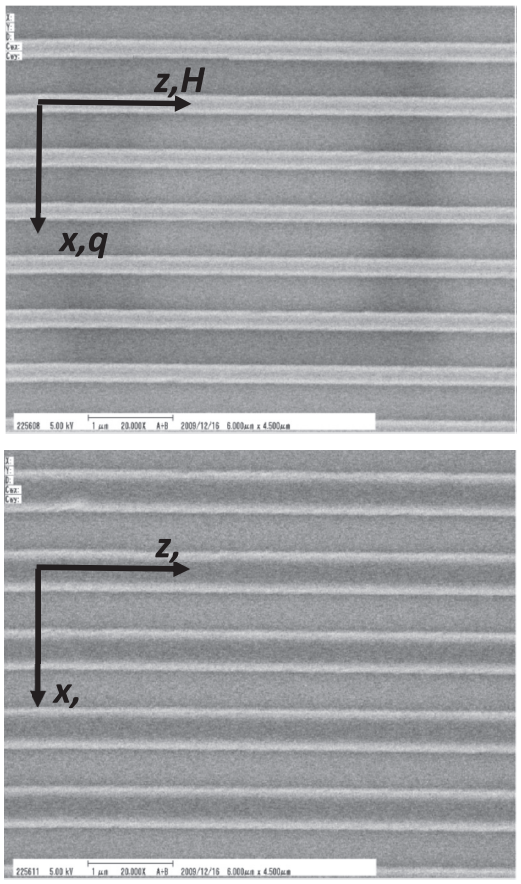

FIG. 2. Scanning electron micrograph of the stripe arrays with different widths $w_n = 150$ nm and $w_w = 400$ nm. The edge-to-edge spacing for all the nanostripe arrays is maintained at 400 nm.

The spectra of thermally excited spin waves have been measured in the backscattering configuration by BLS using a Sandercock-type (3 + 3) pass tandem Fabry–Perot interferometer. A magnetic field $\mu_0 H_0 = 0.03$ T has been applied in the sample and along the stripe lengths while the BLS spectra were recorded by sweeping the spin-wave wave vector (q) with amplitude ranging from 0 to 0.022 nm^{-1}. To this aim, the sample has been mounted on a goniometer to allow rotation around the field direction, i.e. to vary the incidence angle of light θ between 0° and 70°. For the stripe array, q is oriented parallel to the stripe widths (i.e. in the x direction in Fig. 1, which includes the BLS geometry and coordinate axes used in the theory).

III. THEORY

The calculations for the spin-wave spectrum in the interacting stripe arrays are performed using a straightforward generalization of the microscopic dipole-exchange theory described elsewhere[25] for individual (i.e. noninteracting) ferromagnetic stripes, with the external field H_0 here applied along the

stripe lengths (z direction). This type of formalism, which has also been applied to other magnetic nanostructures, such as cylindrical wires[26] and spheres,[27] is particularly appropriate for cases where the magnetization in the array elements may be spatially inhomogeneous. It also avoids introducing assumptions for the effective pinning at boundaries,[28] as often done in macroscopic theories. By contrast with a recent comparison[29] of BLS experiments and theory for Py stripes in closely-spaced horizontal arrays (patterned films), we now extend the theory to include the coupling between stripes for the vertically stacked arrays of interest here.

Briefly, the modified theoretical analysis includes terms in the Hamiltonian for the dynamic and static parts of the interstripe dipolar interactions, as well as the usual intrastripe dipolar and exchange terms. This can be achieved by analogy with recent application of the microscopic theory to other finite nanostructured arrays,[25–27] so details will not be given here. Each stripe in the array is modeled as an infinitely long stripe with appropriate thickness (t or d) and width w. The effective spins are arranged on a simple cubic lattice, with the effective lattice constant a chosen to be comparable with or less than the so-called exchange length (approximately 5.3 nm for permalloy). The Hamiltonian H for the array has three parts, as below:

$$H = \frac{1}{2}\sum_{i,j}\sum_{\alpha,\beta} V_{ij}^{\alpha\beta} S_i^{\alpha} S_j^{\beta} - g\mu_B \sum_i H_0 S_i^z - \sum_i K_i \left(S_i^z\right)^2 . \tag{1}$$

Here, V in the first part describes the interaction between spins $\mathbf{S}_i$ and $\mathbf{S}_j$ at lattice sites i and j, which may be in either the same or a different stripe:

$$V_{ij}^{\alpha\beta} = g^2\mu_B^2\left[\left(|r_{ij}|^2\delta_{\alpha\beta} - 3r_{ij}^{\alpha}r_{ij}^{\beta}\right)/|r_{ij}|^5\right] - J_{ij}\delta_{\alpha\beta}. \tag{2}$$

Following Ref. 25, the interaction contains both the long-range dipole-dipole terms (with $\mathbf{r}_{ij}$ denoting the vector connecting sites i and j) and the short-range exchange terms J_{ij}, while α and β denote Cartesian components. The second and third parts in Eq. (1) describe the Zeeman energy of the applied field H_0 (in terms of the Landé factor g and the Bohr magneton μ_B) and the single-ion anisotropy energy relative to the long axis of the stripes, respectively. The coefficient K_i may be positive or negative (for easy-axis or easy plane anisotropy, respectively); for simplicity, it is assumed to have the value K_{surf} at any surface site of a stripe and the bulk value K_{bulk} otherwise. Although the anisotropy is small in Py, it will be shown that a surface contribution can nevertheless affect the spatial quantization of the modes in the samples with small width w.

As in earlier work,[25] the steps in the theory involve first solving for the equilibrium spin configurations in the array, using an energy minimization procedure appropriate for low temperatures and treating the spins as classical vectors. Then the total Hamiltonian is re-expressed in terms of a set of boson operators, which are defined relative to the local equilibrium coordinates of each spin. Finally, keeping only the terms up to quadratic order in an operator expansion, we solve for the spin-wave excitations of the interacting magnetic stripes. In general, the procedure consists of diagonalizing a $2N \times 2N$ matrix, where N is the total number of effective spins in any transverse (xy) plane of the trilayer array. Since typically $N \sim 5000$ or less, depending on the stripe sizes, this must be done numerically. The coupled modes will depend, in general, on the wave vector k along the longitudinal axis of translational symmetry. With the BLS geometry in the present case (see Fig. 1), we have $k = 0$, but the spin waves also have a variable transverse (along x direction) wave vector q, as discussed earlier.

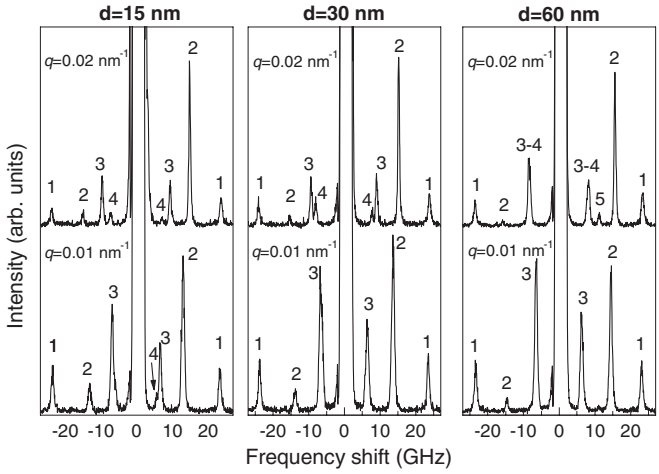

FIG. 3. Couple of BLS spectra measured for $q = 0.01$ and $0.02\ \text{nm}^{-1}$ for trilayer films having different thickness of the middle layer (d). The applied field is $\mu_0 H_0 = 0.03$ T applied in the sample plane.

The theory can also be used to calculate a probability amplitude [obtained from the square root of the total mean-square amplitude, $\langle(m^x)^2\rangle + \langle(m^y)^2\rangle$]. This quantity represents the relative amplitude for each of the discrete spin-wave branches as a function of its wave vector q and the position anywhere in the trilayer system. The calculations are a direct extension of the Green's function approach described elsewhere for single nanostripes.[25,26] The predicted results for the spatial distributions of the modes are used in Sec. IV to interpret the strengths of the peaks occurring in the BLS experiments. The square of the probability amplitude is proportional to a spectral intensity for each spin-wave mode, which should be broadly comparable with the BLS intensity, except we note that the latter quantity incorporates other factors such as the magneto-optical coupling strength, the transmission of the light into and out of the sample, optical absorption, etc.[30] The probability amplitude does not provide information about the relative phases for the modes. The same method has been used to calculate the frequency and spatial profile of spin wave in continuous (unpatterned) trilayer films.

IV. RESULTS

A. Continuous trilayer films

As a first step in our dynamical characterization, we have measured the dispersion relations (frequency vs wave vector) for spin waves in the continuous (unpatterned) Py(30 nm)/Cu(10 nm)/Py(d)/Cu(10 nm)/Py(30 nm) films for different thickness of the middle layer (d). Selected BLS spectra measured for a fixed magnetic field $\mu_0 H_0 = 0.03$ T and two values of q (0.01 and $0.02\ \text{nm}^{-1}$) are shown in Fig. 3. All of these spectra are characterized by the presence

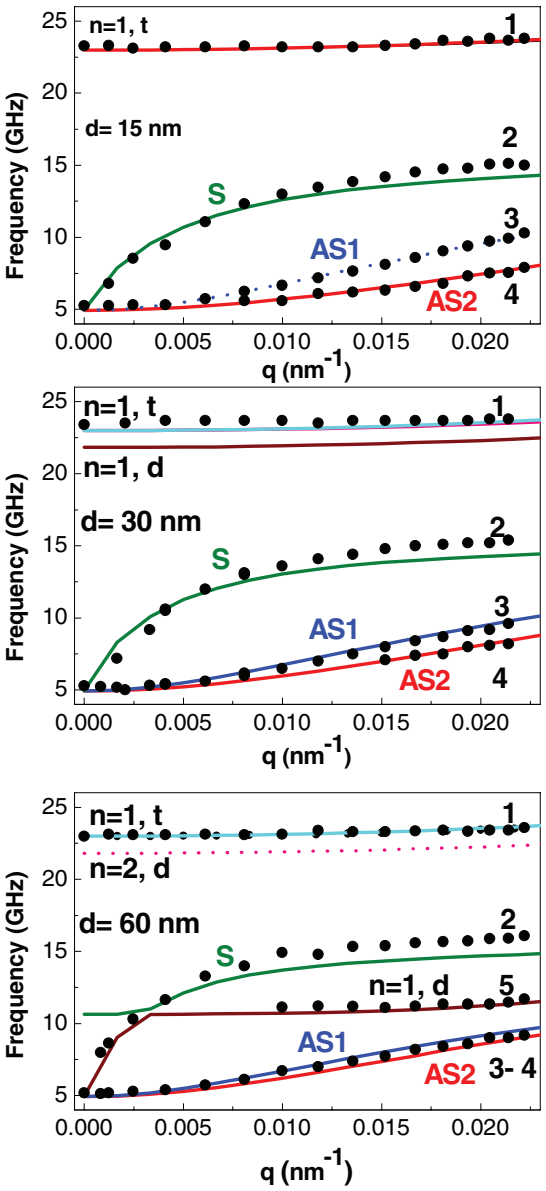

FIG. 4. (Color online) Experimental (points) and calculated spin-wave frequencies for the trilayer films with different thickness of the middle Py layer (d) as a function of the transferred in-plane wave vector q. The applied field is $\mu_0 H_0 = 0.03$ T. The modes are labeled according to the nomenclature described in the text.

of several well-resolved peaks, labeled by integer numbers, whose dispersion and evolution with d is presented in Fig. 4.

Inspection of Figs. 3 and 4, suggests that the common features for all the samples is the presence of one mode (labeled as 1 in the experimental spectra) at about 23.4 GHz, whose frequency is almost constant with q, and a highly dispersive mode (2) in the range between 5 and 15 GHz. The latter is the most intense peak in the measured spectra, and its intensity asymmetry between the Stokes and anti-Stokes sides increases for increasing q.

The main differences between the spectra occur in the low frequency range where two dispersive modes (3 and 4) are detected. The frequency splitting of these modes increases with q and decreases on increasing the thickness of the inner

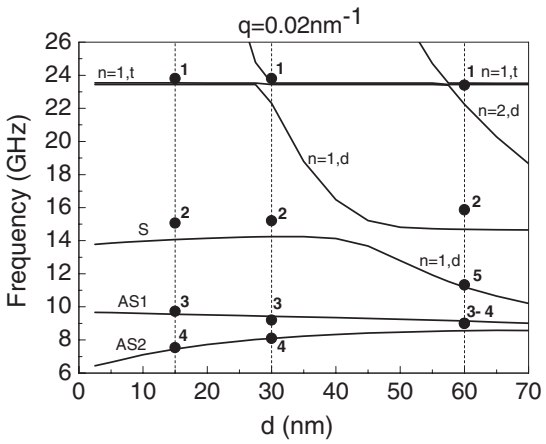

FIG. 5. Calculated frequency for the trilayer films as a function of the thickness d of the middle film and fixed value of $t = 30$ and $d_0 = 10$ nm. The applied field is $\mu_0 H_0 = 0.03$ T and the wave vector is $q = 0.02$ nm^{-1}. Points are the measured frequency taken from Fig. 4. Vertical dotted lines are drawn corresponding to the thickness of the samples investigated in this paper ($d = 15$, 30, and 60 nm).

layer (d) until, for $d = 60$ nm, only one peak is detected. For all the investigated samples, modes 2, 3, and 4 are degenerate in frequency in the limit of q approaching zero. In addition, in the sample with $d = 60$ nm, another dispersionless mode (5) is measured at about 11.5 GHz for q larger than 0.01 nm^{-1}.

To better understand the nature of the detected modes we have calculated, using the theory presented in Sec. III, the frequencies and the profiles of dipolar-exchange spin waves for the studied trilayer films, as shown by the curves plotted in Figs. 4–6. The theoretical predictions are in good, though not perfect, agreement with the experimental results in the whole range of wave vectors investigated. The main discrepancy is represented by fact that the theory underestimates the frequency of the most dispersive mode for $q > 0.008$ nm^{-1} while providing a satisfactory agreement in the low q range.

Figure 5 contains the calculated frequency curves as a function of the thickness of the middle layer (d) and fixed thicknesses of the other layers ($t = 30$ nm and $d_0 = 10$ nm), while Fig. 6 shows the calculated distributions of dynamic magnetization for fixed values of d (15, 30, and 60 nm) and for fixed $q = 0.02$ nm^{-1}.

These calculations were carried out using realistic values for the saturation magnetization $M_s = 0.072$ T, exchange stiffness $D = 35$ T $\cdot$ nm^2, and gyromagnetic ratio $= 29.5$ GHz/T of Py, from which the parameters of the model in Eqs. (1) and (2) can be deduced.[25] Briefly, we have $D = SJa^2$, where the effective lattice parameter a was discussed previously. Also we may express $D = 2A/M_s$ where A is the micromagnetic stiffness parameter. To optimize the fit to the mode at frequency $\sim$23 GHz, which appears in all three structures and is interpreted as a standing mode (see below), we took the outer (top and bottom) film thickness t to be $\sim$29 nm instead of the nominal 30 nm.

Magnetization distributions calculated for all the investigated samples suggest that the doublet of modes (23.43 and 23.54 GHz), which are not resolved in the measured spectra

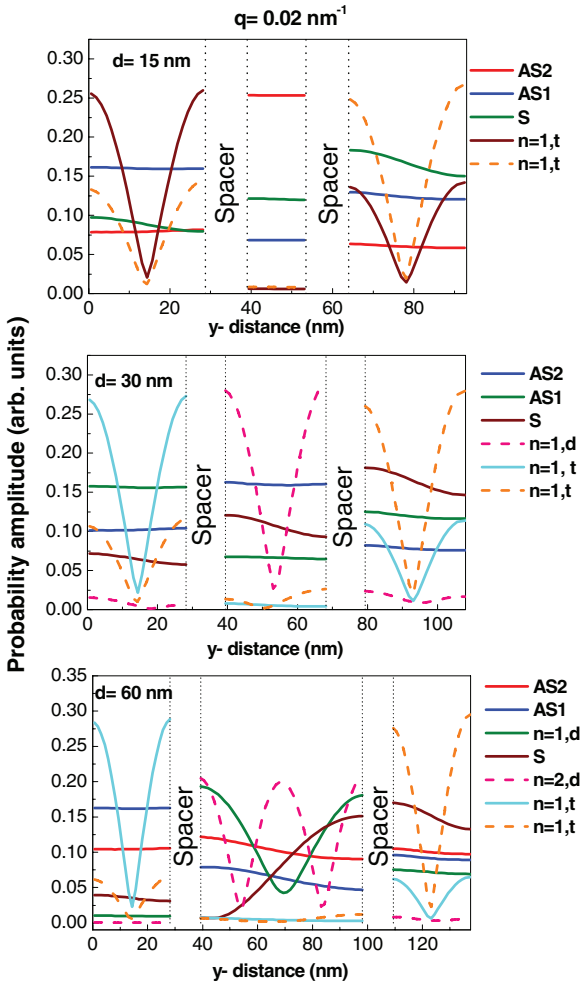

FIG. 6. (Color online) Thickness dependence of the calculated (root mean square) total amplitude of dynamic magnetization for the spin waves reported in Fig. 2. The applied field is $\mu_0 H_0 = 0.03$ T and the wave vector is $q = 0.02$ nm^{-1}.

(mode 1), oscillate across the top and bottom Py films with one nodal plane across their thickness and have an almost vanishing precession amplitude in the middle film. This explains why their frequency does not depend on d in Fig. 5. These modes are analogous to the first perpendicular standing spin wave, denoted as ($n = 1$,t) where the n value is the number of nodes, of an isolated $t = 30$-nm-thick Py film. Here, they are coupled by the dynamic dipolar interaction which removes their frequency degeneracy. It is interesting to notice that these two modes have opposite spin precession amplitude in the two outermost films.

For $d = 30$ and 60 nm, theory also predicts the existence of two modes at slightly lower frequency (21.95 and 21.90 GHz, respectively). As suggested by the calculated spatial profiles, these modes are standing perpendicular waves being mostly localized in the middle Py film with one and two nodal planes, hence denoted as ($n = 1$, d) and ($n = 2$, d), respectively. This is the reason why they are not detected in the BLS spectra in the whole range of wave vectors investigated. As can be seen in Fig. 5, these modes are characterized by the typical $1/d^2$ frequency dependence due to exchange interaction and exhibit repulsion at the crossing point with other modes (for d of about 45 nm with mode S, for example). Mode 5, which we measure in the high q-vector spectra (see Fig. 4) at 11.33 GHz for $d = 60$ nm sample, derives from the first standing perpendicular mode of the middle film ($n = 1$, d). It has a vanishing cross section at low q, being mostly confined in the middle film, while on increasing q, its amplitude significantly increases in the top film, making the mode visible in the measured spectra.

The most dispersive mode, labeled 2 in the experimental spectra, is characterized by an appreciable oscillation of the dynamic magnetization in all three Py films, although additional mode-mixing (hybridization) effects are also evident (e.g. for $d = 60$ nm). The frequency dispersion recalls that of associated with the in-phase precession of the dynamic magnetizations in the two magnetic films for Py/Cu/Py films (the acoustic mode).[9] It corresponds to the Damon–Eshbach[31] mode of the entire stack, which consists of the surface mode of each film and whose envelope function varies exponentially across the sample thickness. For the above-mentioned reason, the calculated dispersion curve of this surface mode will be labeled in the rest of the paper as surface mode S (see profile of mode S in Fig. 6). This mode of surface character is only predicted to exist when the magnetic films are thicker than the nonmagnetic ones, a situation which is always fulfilled in our samples. In addition, the frequency of the S mode is found to be independent of the thickness ratio between magnetic and nonmagnetic films, in agreement with theoretical predictions.[32]

At frequencies below the S mode, there is a couple of modes (labeled 3 and 4 in the experimental spectra) whose dispersion (see Fig. 4) is qualitative similar to that of surface modes with an out-of-phase (i.e. asymmetric) precession of the dynamic magnetization in Py/Cu/Py films.[9] Therefore, we call them as AS1 and AS2 modes. The highest-frequency mode of the doublet is almost insensitive to d, as shown in Fig. 5, while the frequency of the lower-frequency mode increases on increasing d. These two modes represent the dipolar standing modes of the structure, consisting of dipolar modes in each film and whose envelope function varies in an oscillatory way in the direction perpendicular to the sample plane.[32] In the case of a layered structure made up of several magnetic layers, these low-frequency modes would give rise to the band of magnetostatic bulk modes. By looking at the magnetization amplitude reported in Fig. 6, one sees that modes AS1 and AS2 have almost uniform amplitude of the dynamic magnetization in the three Py films with the difference that the mode at lowest (highest) frequency mainly oscillates in the middle (top) film.

To probe the origin of the low-frequency doublet and understand the effect of interlayer dipolar coupling on the different modes, we have plotted in Fig. 7 the calculated frequency dependence as a function of the Cu thickness (d_0) for fixed thickness of the three Py layers at $q = 0.02$ nm^{-1}. For large $d_0 > 150$ nm, when the three magnetic films are far enough apart that they can be considered uncoupled, the frequency of all the modes is constant vs d_0, and the modes of surface character (Damon–Eshbach-like modes) of films with the same thickness are degenerate in frequency (top and bottom film for $d = 15$ nm and $d = 60$ nm, all three films for $d = 30$ nm). For comparison, separate dipole-exchange calculations for single films of Py with thickness 15, 30, and 60 nm lead us to predict Damon–Eshbach-type modes

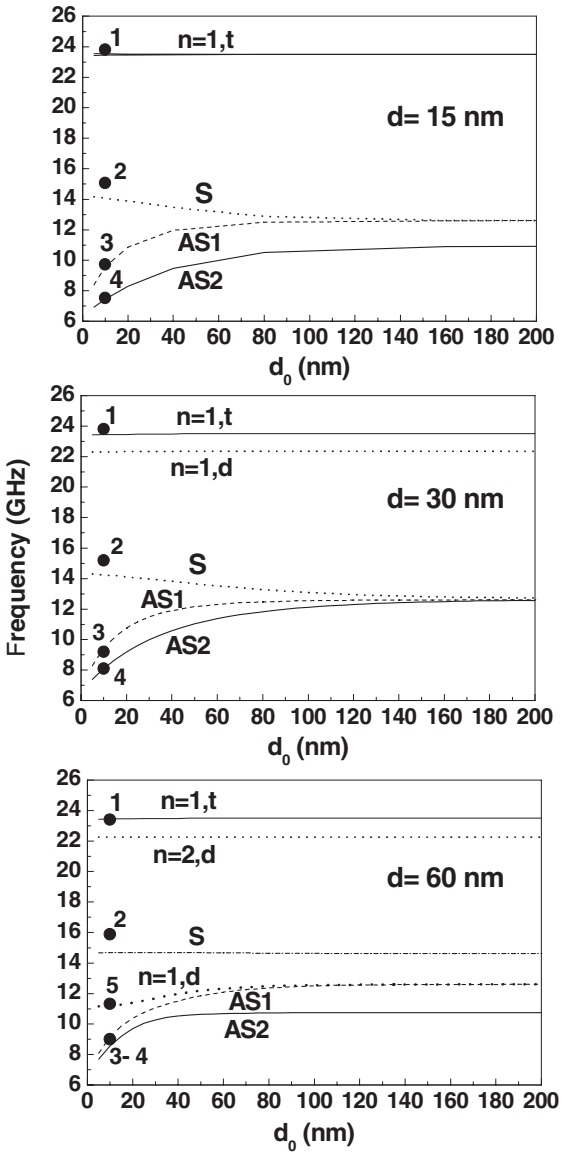

FIG. 7. Frequency dependence of the modes as a function of the thickness of the Cu spacer (d_0) for fixed thickness of the Py films. The applied magnetic field is $\mu_0 H_0 = 0.03$ T and the wave vector is $q = 0.02$ nm^{-1}. Full points are the measured frequency values taken from Fig. 4. Note that the mode labeling is appropriate to the experimental samples where $d_0 = 10$ nm.

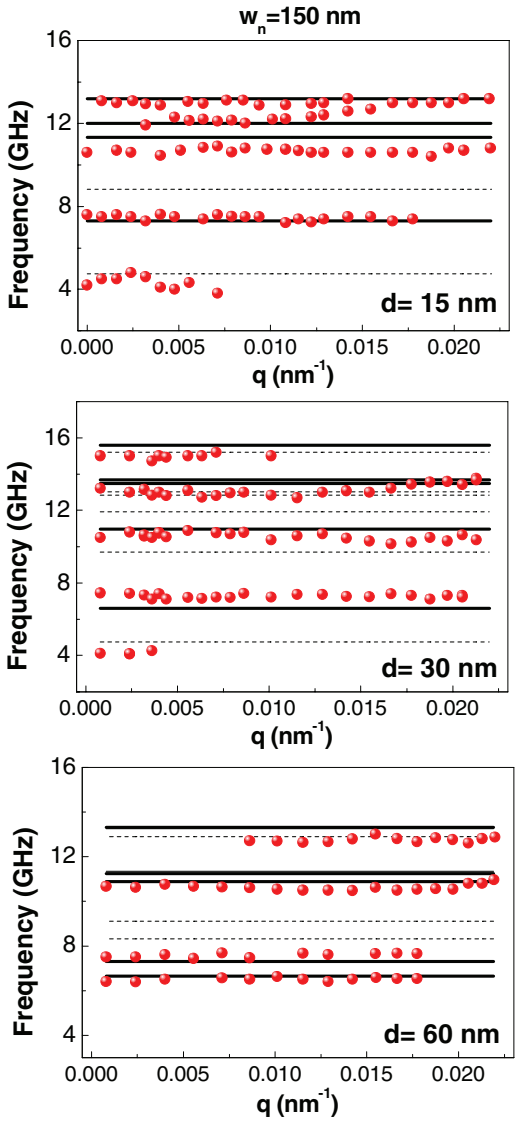

FIG. 8. (Color online) Experimental (points) and calculated (lines) spin-wave frequencies for the 150-nm-wide stripes and different thickness of the middle Py layer (d) as a function of the transferred in-plane wave vector q. The external magnetic field $\mu_0 H_0 = 0.03$ T is applied along the z axis, i.e. along the in-plane easy direction of the stripes. Bold lines represent the calculated modes with largest intensity.

at approximate frequencies of 11.0, 12.7, and 14.6 GHz, respectively.

On reducing d_0, the modes interact through the dipolar stray field associated with the precessing magnetization, which lifts their degeneracy, and the modes present a different frequency evolution. In particular, mode S experiences an upwards frequency shift on reducing d_0 for samples with $d = 15$ and 30 nm, while it is constant for $d = 60$ nm. In the limiting case of vanishing thickness of the Cu spacer (d_0), it becomes the Damon–Eshbach mode of a single magnetic film having a total thickness of $2t + d$. Analogous results have been found by Emtage *et al.*[33] For the doublet of modes AS1 and AS2, the magnetization of the middle Py film is expected to precess out of phase with respect to one or both the outermost films (top or bottom). The frequency of these modes decreases on reducing d_0. This happens because the modes are largely sensitive to the dipolar coupling which depends on the interlayer distance d_0. In the limiting case of vanishing spacer thickness, they merge into the bulk-type magnetostatic modes. For all the investigated samples, the high-frequency modes (above 20 GHz), being modes resonating across the film thicknesses, are independent of d_0 and can be considered as uncoupled because the dipolar stray field they generate outside the films is negligible.

B. Trilayer stripes $w_n = 150$ nm

Different from the case of the plane multilayered film analyzed above, when the BLS technique is applied to the study

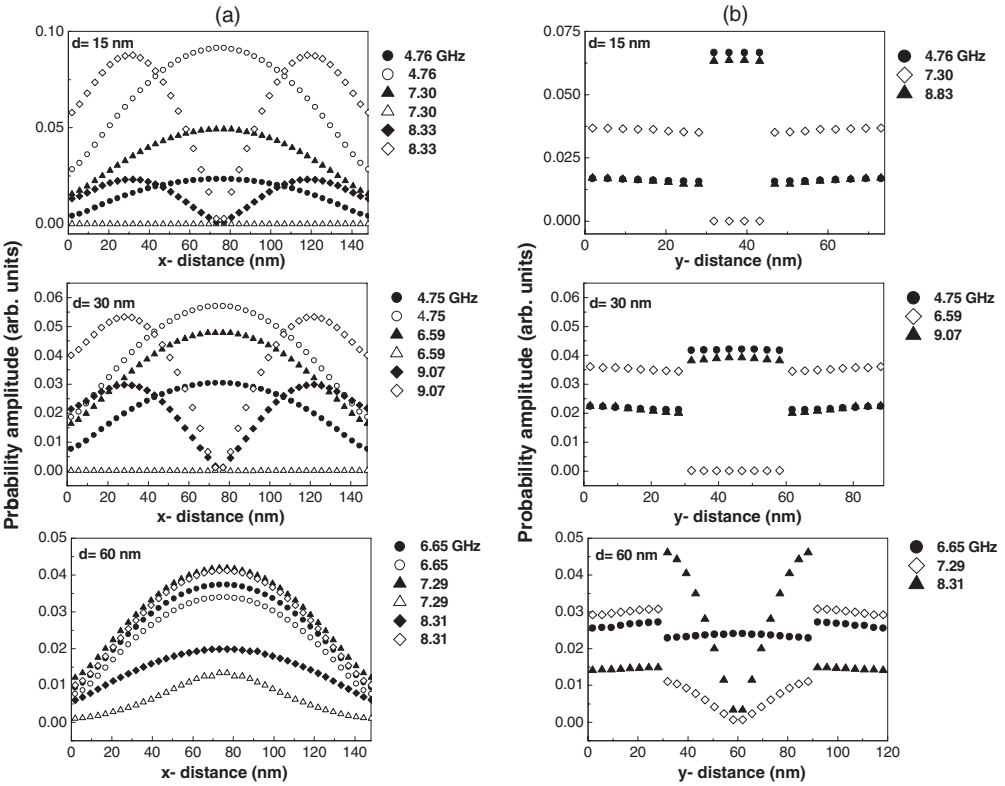

FIG. 9. Spatial distribution of the lowest-frequency modes for different thickness of the middle layer d calculated (a) along the stripe widths and (b) along the thickness of the Py stripes. The stripes are 150 nm wide, and a magnetic field $\mu_0 H_0 = 0.03$ T is applied along the z direction. In (a), full (open) points refer to the outermost (middle) Py layer.

of the array of stripes, the measured spectra exhibit a rather large number of modes, resulting from the lateral quantization. In Fig. 8, we report the comparison between the measured and calculated spin-wave frequency dispersion for the stripes having width $w_n = 150$ nm and different thickness of the middle Py layer (d). Here, we show results in the frequency range up to 16 GHz because the highest-frequency mode measured for the continuous trilayer films (corresponding to mode 1 in the spectra of Fig. 3) is unaffected by the patterning, and its frequency remains constant at about 23.4 GHz. As a consequence of the lateral confinement within the stripes width, the BLS spectra of the stripes consist of several discrete peaks, whose frequency does not change as a function of the wave vector q. The lines are the results of calculations, and we have marked as continuous bold lines the modes expected to have larger BLS intensities.

In making these fits, we employed the same gyromagnetic ratio and M_s parameters as before for the reference films, but the exchange stiffness D was reduced to 25 T nm^2 for $d = 15$ nm, resulting in a better fit to experiment for this sample. Also, a small single-ion anisotropy (negligible for the complete films, but now attributable to the lateral edges of the thin stripes) was introduced corresponding to an average $SK/g\mu_B = -0.016$ T, which is similar to the value deduced previously for Py nanostripes.[34] An overall good agreement is obtained between measured and calculated frequencies for all the stripes with different thickness of the middle layer. Slight discrepancies can be ascribed to the fact that, in the calculation, we have assumed a perfectly symmetric structure, while in the real sample, the dynamical properties of the top stripes can be different because of the presence of the free surface and the consequent oxidation. For the $d = 15$ and 30 nm stripes, the lowest-frequency mode at about 4 GHz is only detected in the region of low wave vectors, while for $d = 60$ nm, the lowest-frequency mode is at higher frequency (6.4 GHz), and it is measured in the whole q range investigated.

To identify the nature of the observed modes, we present in Fig. 9 the calculated total amplitude of dynamic magnetization for the three lowest-frequency modes across the stripe widths (x-direction dependence, with averaging in the y direction) and along the direction of the stripe stack (y-direction dependence, with averaging in the x direction). The calculated spatial profiles across the stripe width are typical of standing wave resonance modes existing in longitudinally magnetized stripes (saturation magnetization parallel to the stripe lengths) and can be considered as the superposition of travelling Damon–Eshbach waves propagating in opposite direction within the stripes.[35] A common feature for all the layered stripes is that many modes occur as doublets which are degenerate in frequency, essentially because of symmetric and antisymmetric combinations involving the top and bottom layers. There is no noticeable difference between the spatial distribution for the $d = 15$ nm and $d = 30$ nm samples, with the magnetization amplitude which does not change significantly across the sample thickness, as can be inferred from inspection of Fig. 9. The second-lowest frequency modes, mainly localized in the top stripes and negligible precession amplitude in the middle stripe, are characterized by a nearly

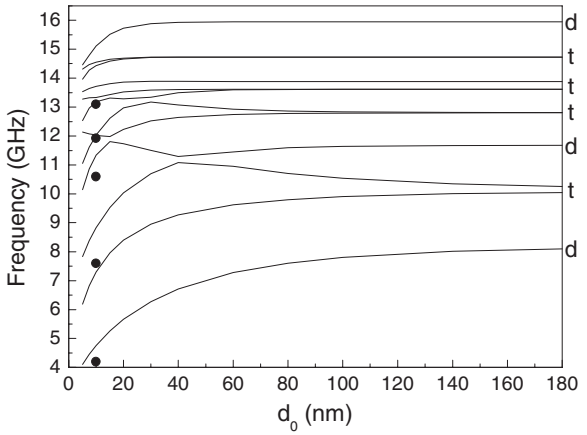

FIG. 10. Frequency dependence of the modes as a function of the thickness of the Cu spacer (d_0) for layered stripes with $d = 15$ nm and $q = 0.02$ nm^{-1}. Full points are the measured frequency values taken from the upper panel of Fig. 8. Labels d and t indicate the stripe (middle, d) and (outermost, t) where the modes are localized for large d_0 values.

uniform precession amplitude across the stripe width and can be considered as the quasiuniform (fundamental) modes of the stripes. By contrast, the third mode is confined in the middle stripe and has one nodal plane along the stripe thicknesses.

For $d = 60$ nm, the profile of the three lowest frequency modes are quasiuniform and have comparable amplitude in both the outer and middle stripes. The most significant difference with respect to the $d = 15$ nm and $d = 30$ nm layered stripes is represented by the fact that the lowest frequency mode (6.65 GHz) is at a significantly higher frequency value compared with the other samples, in agreement with our experimental findings. This might be attributable to single-ion anisotropy effects at the lateral edges of the middle layer when $d = 60$ nm. Another interesting feature is that the dynamical magnetization for modes at 7.29 and 8.31 GHz has one nodal plane across the thickness of the middle layer, meaning that they originate from the mode measured for the continuous trilayer film at 10.7 GHz (mode 5 of Fig. 4), whose character is that of a standing spin wave across the thickness of the middle layer.

Similarly to what was presented in Fig. 7 for the trilayer films, in Fig. 10, we show the calculated frequency for the stationary modes in layered stripes with $d = 15$ nm and width $w_n = 150$ nm, as a function of the thickness of the Cu spacer (d_0). This graph illustrates that the modes detected for the stripes, in our samples $d_0 = 10$ nm, come for modes that for large d_0 values (uncoupled stripes) are localized either in the middle (d) or outer stripes (t). Even in this case, the dipolar coupling determines a frequency reduction (increase), for modes with out-of-phase (in-phase) precession of dynamic magnetization in the different films and repulsion at crossing points.

C. Trilayer stripes $w_n = 400$ nm

Similarly to what has been done for the narrower stripes ($w_n = 150$ nm), in Fig. 11, we present the comparison between the measured and calculated frequency dispersion (frequency

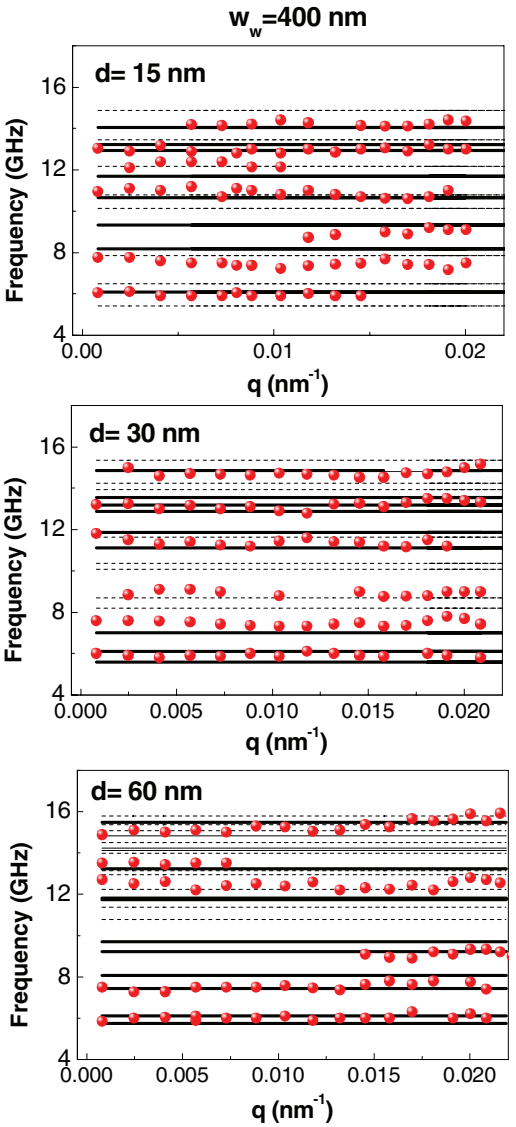

FIG. 11. (Color online) Experimental (points) and calculated (lines) spin-wave frequencies for the 150-nm-wide stripes and different thickness of the middle Py layer (d) as a function of the transferred in-plane wave vector q. The external magnetic field $\mu_0 H_0 = 0.03$ T is applied along the z axis, i.e. along the in-plane easy direction of the stripes.

vs wave vector) for the $w_w = 400$-nm-wide layered stripes for different values of d.

Here, the spectra are richer in terms of the number of stationary modes detected in the spectra, due to the larger stripe widths, which can accommodate more stationary modes in the frequency range of interest with respect to the previous case $w_n = 150$ nm. A good agreement between the experiment and the calculated frequencies is obtained, especially if one considers the most intense modes, i.e. those which are characterized by the largest intensity in the BLS spectra. Inspection of mode profiles presented in Fig. 12 suggest that, even for this width, the modes appear in doublets whose frequency, mode amplitudes, and localizations in the three Py layers are similar to those calculated for the narrower stripes ($w_n = 150$ nm). The principal difference worth mentioning is the case of

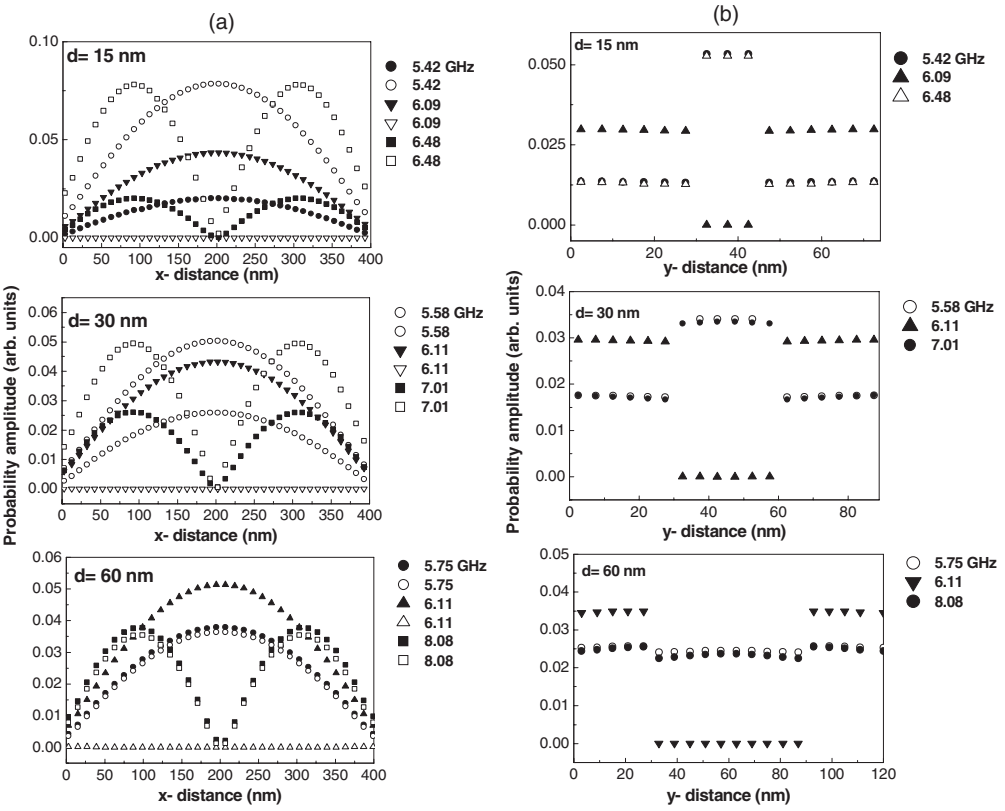

FIG. 12. (a) Spatial distribution of the three lowest frequency modes for different thickness of the middle layer d calculated along the stripes width and (b) along the thickness of the sample. The stripes are 400 nm wide, and a magnetic field $\mu_0 H_0 = 0.03$ T is applied along the z direction. In (a), full (open) points refer to the top (middle) Py layer.

$d = 60$ nm, where the higher-frequency doublet (at 8.08 GHz) has one nodal plane across x distance (the stripe width), whereas the corresponding doublet (at 8.31 GHz) is almost uniform for $w_n = 150$ nm, as seen in Fig. 9. This situation is inverted if one looks at the profiles of the two doublets along the trilayer thickness (y distance), where the mode amplitude for the case of $w_n = 150$ nm stripes exhibits one nodal plane in the y direction.

V. CONCLUSIONS

In this paper, we have comprehensively studied, both theoretically and experimentally, dipole-exchange spin waves in a layered structure consisting of three ferromagnetic permalloy films separated by Cu films, for three different thicknesses of the middle permalloy film ($d = 15$, 30, and 60 nm). The modes detected by Brillouin light scattering experiments have been classified, on the basis of the microscopic dipole-exchange theory, as follows:

(i) Perpendicular standing modes (resonating through the thickness of the elemental layers) which occur in the high-frequency range and have the same frequency both in the continuous films and stripes (i.e. they are unaffected by patterning).

(ii) Surface and bulk modes of the stack, which are constituted by dipolar surface modes of the elemental layer and have, respectively, an exponential or an oscillating envelope across the stack.

With the above information in hand, we have performed a systematic investigation of spin waves confined within stripes of different widths ($w_n = 150$ nm and $w_w = 400$ nm), fabricated by nanolithography starting from the same multilayered stack. A number of discretized modes with different spatial localization across the width of the stripes and across the layered structure have been detected. Both the frequencies and the cross sections of the measured BLS peaks are in reasonable agreement with the results of the microscopic theory, enabling us to describe the spatial distribution of the modes. We believe that this work will be useful for the design, tailoring, and exploitation of multilayered spintronic devices where the role of magnetic normal modes in the GHz range of frequency can be relevant.

This work was partially supported by MIUR-PRIN 2010-11 Project2010ECA8P3 “DyNanoMag”.

[1] P. Grünberg, in *Light Scattering in Solids V*, edited by M. Cardona and G. Güntherodt (review), Topics in Appl. Phys. Vol. 66 (Springer, Berlin, 1989).

[2] *Spin Dynamics in Confined Magnetic Structures III*, edited by B. Hillebrands and A. Thiaville (Springer, Berlin, 2006).

[3] *Spin Wave Confinement*, edited by S. O. Demokritov (Pan Stanford, Singapore, 2008).
[4] S. I. Kiselev, J. C. Sankey, I. N. Krivorotov, N. C. Emley, M. Rinkoski, C. Perez, R. A. Buhrman, and D. C. Ralph, Phys. Rev. Lett. **93**, 036601 (2004).
[5] A. Yamaguchi, A. Fukushima, H. Kubota, and S. Yuasa, IEEE Trans. Magn. **48**, 2816 (2012).
[6] F. Montoncello, L. Giovannini, F. Nizzoli, R. Zivieri, G. Consolo, and G. Gubbiotti, J. Magn. Magn. Mater. **322**, 2330 (2010).
[7] G. Consolo, B. Azzerboni, G. Gerhart, G. A. Melkov, V. Tiberkevich, and A. N. Slavin, Phys. Rev. B **76**, 144410 (2007).
[8] F. Montoncello, L. Giovannini, F. Nizzoli, H. Tanigawa, T. Ono, G. Gubbiotti, M. Madami, S. Tacchi, and G. Carlotti, Phys. Rev. B **78**, 104421 (2008).
[9] G. Gubbiotti, M. Kostyleva, N. Sergeevaa, M. Conti, G. Carlotti, T. Ono, A. N. Slavin, and A. Stashkevich, Phys. Rev. B **70**, 224422 (2004).
[10] G. Gubbiotti, M. Madami, S. Tacchi, G. Carlotti, H. Tanigawa, and T. Ono, J. Phys. D: Appl. Phys. **41**, 134023 (2008).
[11] G. Gubbiotti, M. Madami, S. Tacchi, G. Carlotti, and T. Okuno, Phys. Rev. B **73**, 144430 (2006).
[12] V. V. Naletov, G. de Loubens, G. Albuquerque, S. Borlenghi, V. Cros, G. Faini, J. Grollier, H. Hurdequint, N. Locatelli, B. Pigeau, A. N. Slavin, V. S. Tiberkevich, C. Ulysse, T. Valet, and O. Klein, Phys. Rev. B **84**, 224423 (2011).
[13] M. Madami, S. Tacchi, G. Gubbiotti, G. Carlotti, H. Pandana, R. D. Gomez, H. Tanigawa, and T. Ono, J. Appl. Phys. **104**, 063510 (2008).
[14] F. Montoncello, L. Giovannini, and F. Nizzoli, J. Appl. Phys. **105**, 07E304 (2009).
[15] Y. Ando, Y. Min Lee, T. Aoki, T. Miyazaki, H. Schultheiss, and B. Hillebrands, J. Magn. Magn. Mater. **310**, 1949 (2007).
[16] A. Helmer, S. Cornelissen, T. Devolder, J. V. Kim, W. van Roy, L. Lagae, and C. Chappert, Phys. Rev. B **81**, 094416 (2010).
[17] P. Vavassori, V. Bonanni, A. Busato, G. Gubbiotti, M. Madami, A. O. Adeyeye, S. Goolaup, N. Singh, C. Spezzani, and M. Sacchi, J. Appl. Phys. **103**, 07C512 (2008).
[18] D. V. Berkov and N. L. Gorn, J. Appl. Phys. **103**, 053908 (2008).
[19] M. Madami, S. Tacchi, G. Gubbiotti, V. Bonanni, D. Bisero, P. Vavassori, A. O. Adeyeye, S. Goolaup, N. Singh, and C. Spezzani, J. Appl. Phys. **105**, 07C115 (2009).
[20] J. Ben Youssef and A. Layadi, J. Appl. Phys. **108**, 053913 (2010).
[21] K. S. Buchanan, K. Yu. Guslienko, A. Doran, A. Scholl, S. D. Bader, and V. Novosad, Phys. Rev. B **72**, 134415 (2005).
[22] X. Zhu, Z. Liu, V. Metlushko, and M. R. Freeman, *Proceedings of the International Conference on Electromagnetics in Advanced Applications, Torino, Italy* (IEEE, Piscataway, NJ, 2007), p. 613.
[23] A. Awad, A. Lara, V. Metlushko, K. Y. Guslienko, and F. G. Aliev, Appl. Phys. Lett. **100**, 262406 (2012).
[24] N. Locatelli, V. V. Naletov, J. Grollier, G. de Loubens, V. Cros, C. Deranlot, C. Ulysse, G. Faini, O. Klein, and A. Fert, J. Appl. Phys. Lett. **98**, 062501 (2011).
[25] H. T. Nguyen, T. M. Nguyen, and M. G. Cottam, Phys. Rev. B **76**, 134413 (2007).
[26] T. M. Nguyen and M. G. Cottam, Phys. Rev. B **72**, 224415 (2005).
[27] H. T. Nguyen and M. G. Cottam, Surf. Rev. Lett. **15**, 727 (2008).
[28] K. Yu. Guslienko and A. N. Slavin, Phys. Rev. B **72**, 014463 (2005).
[29] S. Tacchi, M. Madami, G. Gubbiotti, G. Carlotti, S. Goolaup, A. O. Adeyeye, H. T. Nguyen, and M. G. Cottam, J. Appl. Phys. **105**, 07C102 (2009).
[30] L. Giovannini, R. Zivieri, G. Gubbiotti, G. Carlotti, L. Pareti, and G. Turilli, Phys. Rev. B **63**, 104405 (2001).
[31] R. W. Damon and J. R. Eshbach, J. Phys. Chem. **19**, 308 (1961).
[32] R. E. Camley, T. S. Rahman, and D. L. Mills, Phys. Rev. B **27**, 261 (1983).
[33] P. R. Emtage and Michael R. Daniel, Phys. Rev. B **29**, 212 (1984).
[34] T. M. Nguyen, M. G. Cottam, H. Y. Liu, Z. K. Wang, S. C. Ng, M. H. Kuok, D. J. Lockwood, K. Nielsch, and U. Gösele, Phys Rev. B **73**, 140402(R) (2006).
[35] J. Jorzick, S. O. Demokritov, C. Mathieu, B. Hillebrands, B. Bartenlian, C. Chappert, F. Rousseaux, and A. N. Slavin, Phys. Rev. B **60**, 15194 (1999).